Impedance-Based Stability Evaluation of Virtual Synchronous Machine Implementations in Converter Controllers

Conference Paper · May 2018

DOI: 10.23919/IPEC.2018.8507905

CITATIONS
0

READS
210

5 authors, including:

Eneko Unamuno
Mondragon Unibertsitatea
12 PUBLICATIONS **124** CITATIONS
SEE PROFILE

Atle Rygg
Norwegian University of Science and Technology
43 PUBLICATIONS **235** CITATIONS
SEE PROFILE

Mohammad Amin
Illinois Institute of Technology
30 PUBLICATIONS **212** CITATIONS
SEE PROFILE

Marta Molinas
Norwegian University of Science and Technology
337 PUBLICATIONS **4,038** CITATIONS
SEE PROFILE

Impedance-based Stability evaluation of Virtual Synchronous Machine implementations in Converter Controllers

Eneko Unamuno[1*], Atle Rygg[2], Mohammad Amin[3], Jon Are Suul[2,4], Marta Molinas[2], Jon Andoni Barrena[1]
1 Electronics and Computer Science Department, Mondragon Unibertsitatea, Arrasate-Mondragón, Spain
2 Department of Engineering Cybernetics, Norwegian University of Science and Technology, Trondheim, Norway
3 Electrical and Computer Engineering, Illinois Institute of Technology, Chicago, United States
4 SINTEF Energy Research, Trondheim, Norway
*E-mail: eunamuno@mondragon.edu

***Abstract*—This paper presents a stability evaluation of two Virtual Synchronous Machines (VSM) in the control of Voltage Source Converters (VSCs): the current-controlled (CCVSM) and the voltage-controlled (VCVSM) version of the VSM. The performances of the two control implementations are analyzed under power reference and grid frequency variations and the evaluation of their stability properties is carried out by adopting the impedance-based stability analysis. The results of the *dq* impedance analysis of the two VSMs implementations reveal a clear differentiation between the CCVSM and the VCVSM, particularly in the very low frequency range, even if a close similarity is observed in the time domain responses. The *dq* impedances of both implementations show an *RL* behaviour in the medium frequency range, but when inspecting the stability margin on the Nyquist plot, the VCVSM appears to have a lower stability margin than the CCVSM from the intersection with the unit circle.**

***Index Terms*—Frequency Control, Small-Signal Stability, Synchronous Machine Emulation, Swing Equation, Virtual Synchronous Machine.**

I. Introduction

The increasing penetration of converter-interfaced generation, energy storage systems (ESS) and loads is changing the behavior of power systems that were originally dominated by synchronous machines (SMs) with high values of inertia [1]. The distributed nature of these devices is shifting the structure of electric grids from a classical centralized/top-down structure towards a more decentralized configuration [2], [3]. Although this transition provides several advantages—e.g. a reduction of the dependency on fossil fuels or an alternative to supply the increasing worldwide energy demands—it also poses several challenges to be addressed in order to ensure an adequate operation.

For instance, a higher amount of converter-interfaced systems on an electric grid may cause instabilities in the voltage or frequency because, unlike classical SMs, they do not provide any inherent inertia over power variations [1]. Therefore, these converters must be controlled by more advanced techniques in order to support the grid by providing this inertial behavior and primary reserve—i.e. becoming grid-forming systems instead of merely being grid-following devices [4].

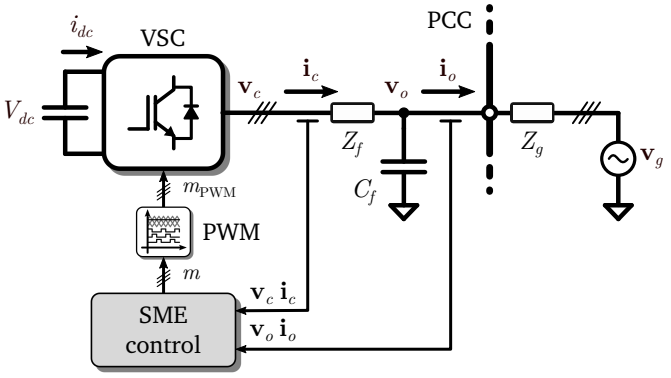

Fig. 1: Configuration of a VSC with synchronous machine emulation control.

In this context, in the last decades synchronous machine emulation (SME) techniques have arisen as one of the most interesting alternatives. These techniques not only provide synthetic inertia to the grid, but they are also capable of operating in a distributed manner as classical SMs, which makes them suitable for both grid-connected or isolated systems. By employing only local measurements, SME controlled converters share power variations occurring in the grid without any extra communication network. Furthermore, some SME control types provide better flexibility when connecting to electric grids by eliminating the dedicated synchronization unit (phase-locked loop or PLL) [5], [6].

Fig. 1 shows a typical configuration of a SME-controlled system, which consists of a voltage-source converter (VSC) connected to the grid through a passive filter, and is controlled based on its local measurements.

In the literature there is a wide variety of SME techniques, and some of them have been already reviewed for instance by D'Arco *et al.* or Bevrani *et al.* in [7] and [8], respectively. In this case, we focus the analysis on the so-called virtual synchronous machines (VSMs), which have been widely employed for different applications such as vehicle-to-grid applications [9] or microgrids [10]–[13]. VSM techniques

can be classified in two main groups:

- Current-controlled virtual synchronous machines (CCVSM) [5], [10], [14]–[16]
- Voltage-controlled virtual synchronous machines (VCVSM) [9], [12], [13], [17]

The aim of this paper is to carry out a comparative evaluation in terms of performance and stability of non-augmented versions of these two types of VSM techniques controlling a grid-connected VSC as the one shown in Fig. 1. By non-augmented we refer to the basic structure of VSM controllers without any feed-forward terms or active damping loops.

In this context, in Section II we first revisit the structure of the two types of VSM techniques and their most relevant characteristics, discussing some of their advantages and drawbacks. Based on these configurations, in Section III we introduce the methodology followed to derive the small-signal state-space models in the *dq*-domain. Moreover, we highlight the importance of rotating impedance matrices so that analytical and measured impedances are compared in the same rotating reference frame.

Following the steps on this methodology, in Section IV we evaluate the performance of each VSM technique in time-domain simulations under different perturbations. Here, we analyze the response of the derived small-signal models and compare them to the non-linear systems, which allows us to verify the analytical models for subsequent analyses.

Section V covers the analysis and comparison of the stability of these systems to identify the advantages and drawbacks of each technique. Although there is a wide variety of methods for determining the stability of such systems, several challenges arise due to the non-linearities of the control strategies. In this work we adopt the impedance-based stability analysis, applying the generalized Nyquist criterion (GNC), which is one of the most used methods to determine the stability of power electronics-based power systems [18]–[22]. Finally, Section VI concludes with the most important remarks of the research.

II. Background and Overview of VSM Control Strategies

VSM techniques are inspired by the concept of operation of classical synchronous machines, which are employed to regulate frequency and voltage of the electric grid. In this context, VSMs usually include an active power controller (APC) that is typically composed by a p/f droop regulator and an inertia-emulation part controlling the output frequency of the converter. Moreover, these techniques integrate a reactive power controller (RPC) that regulates the voltage amplitude through a q/v droop regulator. In the following sections we revise the specific characteristics of CCVSM and VCVSM control strategies, showing their main differences.

A. Current-Controlled Virtual Synchronous Machine

From the two approaches, CCVSMs are the closest to classical SM-based systems because, in addition to the already mentioned active and reactive power controllers, they implement a virtual electrical model of a SM in the control strategy. The CCVSM technique analyzed in this paper is based on the recent study carried out by Mo *et al.* in [5], where two different SM electrical models are compared: a dynamic electrical model and a quasi-stationary model. For the sake of simplicity, in this case we have implemented the dynamic model shown in [5], which is illustrated in Fig. 2.

The active power controller is composed by a droop regulator and the emulation of inertia, which is done by integrating the *swing equation* of classical SMs. The difference of this APC compared to other approaches is that, instead of estimating the frequency of the grid with a PLL, the frequency is generated by filtering the value obtained in the inertia-emulation, assuming that it will vary very slowly. Another difference resides in the fact that the RPC includes a PI regulator to establish the voltage amplitude reference of the virtual SM in the d axis.

Apart from these controllers and the dynamic model of the SM, CCVSMs include a classical current control based on PI regulators with decoupling terms. As shown in Fig. 2, we divide the voltage references obtained in this current controller by the voltage of the dc bus. The purpose is to take into account the oscillations of this bus in the regulation of the converter. However, in this paper we are considering a constant bus voltage, so this division will not have any effect in the following results.

The main advantage of this control is that it increases the flexibility to adapt the behaviour of the converter by varying not only the virtual-inertia but also the windings of the SM model. In addition, the integration of a current controller enables the direct limitation of the current, and there is no need to employ any synchronizing algorithm because the frequency is internally generated.

One of the drawbacks might be the fact that the SM dynamic model must be carefully designed to ensure an adequate dynamic behaviour of the converter.

B. Voltage-Controlled Virtual Synchronous Machine

As shown in Fig. 3, VCVSM techniques are more complex than the previous approach. They have been widely employed in the literature, specially by D'Arco *et al.* for different applications such as microgrids or electric vehicles [9], [12].

The configuration illustrated in Fig. 3 is composed of a cascaded current and voltage controller, a virtual *RL* impedance and similar active and reactive power controllers as in the previous technique.

The PLL, illustrated in Fig. 4, consists of a classical PI regulating the q axis term of the output voltage to zero.

One of the advantages of this technique is that the cascaded current and voltage loops enable the current limitation and the accurate control of the voltage at the output of the converter. In addition, the included virtual-impedance provides more degrees of freedom to adjust the dynamic behaviour of the converter.

However, this specific approach brings about some drawbacks. On the one hand, the high number of cascaded con-

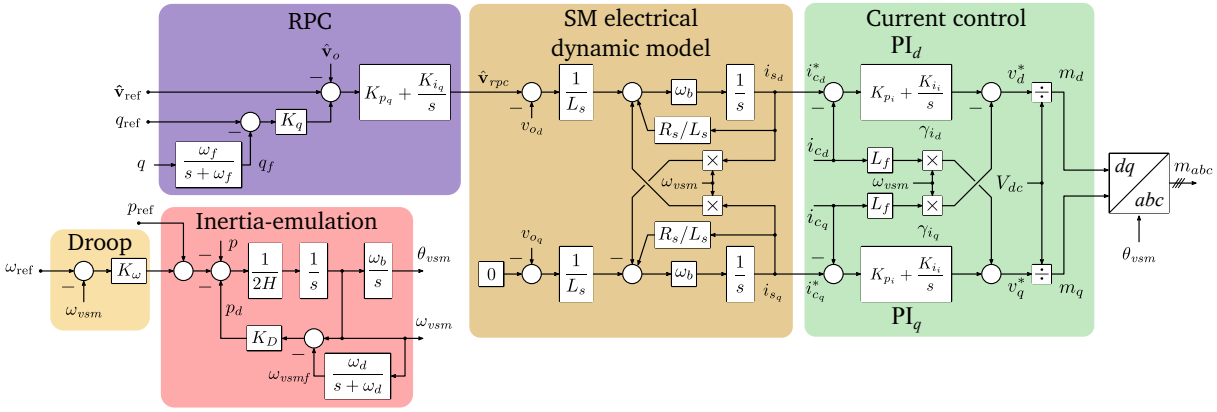

Fig. 2: Current-controlled virtual synchronous machine control diagram based on [5].

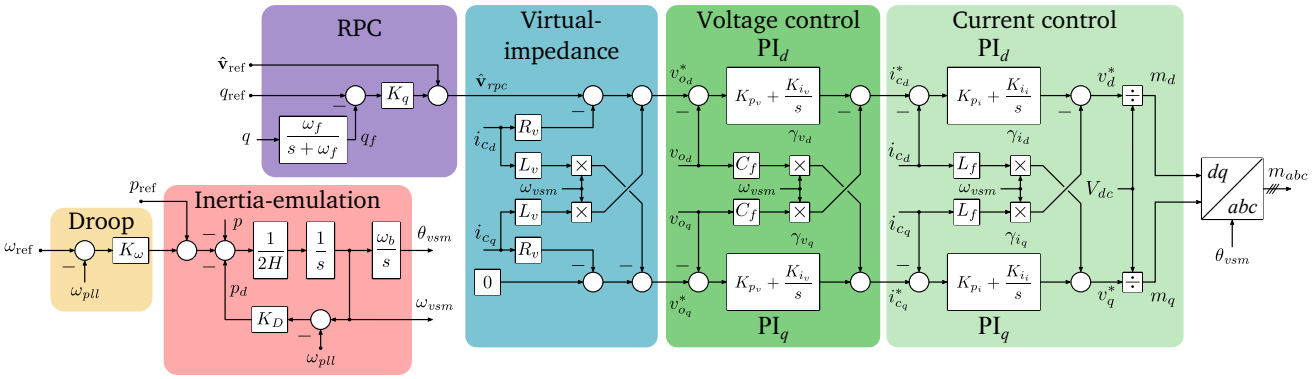

Fig. 3: Voltage-controlled virtual synchronous machine control diagram based on [12].

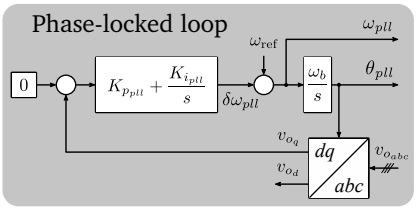

Fig. 4: Structure of the PLL employed for the VCVSM control strategy.

trollers significantly increases the complexity of the technique, making the tuning and configuration of parameters a challenging task. In addition, the strategy shown in Fig. 3, which is based on [12] requires a synchronizing algorithm to capture the frequency of the grid, which could lead to oscillations or stability issues due to the delay of the PLL. In any case, we could avoid the use of a PLL by generating the frequency internally as in the CCVSM. As we are focusing this paper on previous studies of the literature, we leave this analysis for further research activities.

III. Methodology and Simulation Conditions

In order to carry out the performance and stability comparative evaluation, we have developed a methodology that is summarized in Fig. 5.

In this approach, we first derive the differential equations that define the dynamics of the analyzed system, including physical elements as well as control algorithms. Taking into account that some of the differential equations are non-linear, we solve the system to obtain the linearization point $\bar{x}$. This is equal to the steady-state point of operation, and is computed by eliminating the derivative terms and solving the set of equations for specific input values. We then obtain the small-signal state-space model linearized over $\bar{x}$ employing Taylor series expansion, which enables the use of linear techniques for stability analyzes. In order to verify the small-signal model and observe its dynamic performance, we compare it with the non-linear model in time-domain simulations for different disturbances. This part is covered in detail in Section IV. Once the model is verified, we obtain the analytical and measured impedance of each system and analyze the stability applying the GNC.

In this paper all the equations employed to model the VSM-controlled converters are represented in rotating reference frames—i.e. in the *dq* domain—by applying the amplitude-invariant Park transform. In this sense, we can distinguish three main rotating reference frames:

1) Global reference frame (GRF): the d axis of the GRF is aligned with the grid voltage vector v_g, and the q axis, as in the rest of rotating reference frames, leads the d axis

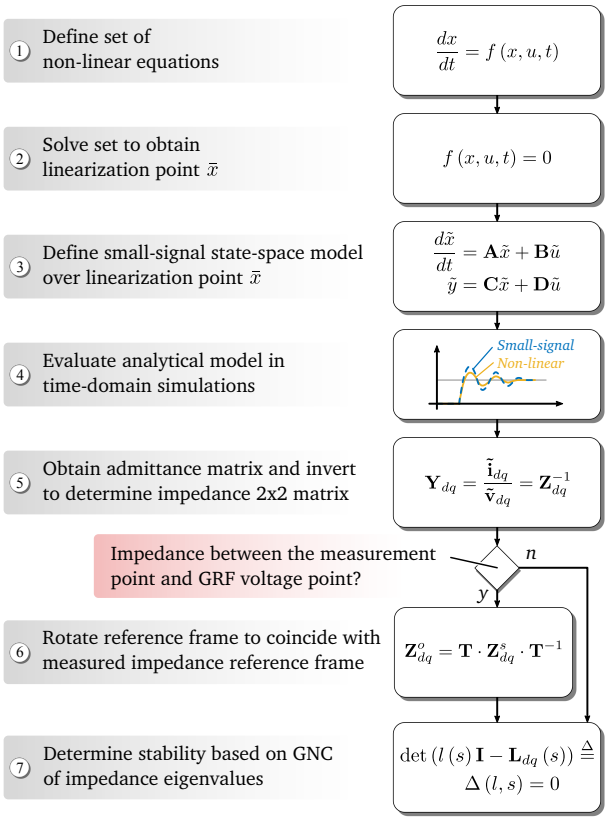

Fig. 5: Methodology for the analytical derivation of *dq* impedance 2×2 matrices and stability analyses based on GNC.

by 90°. The variables referenced to this rotating frame are denoted with superscript "*G*".

2) Local reference frame (LRF): the *d* axis of the LRF is aligned with the output voltage vector v_o. In this case, this voltage corresponds to the voltage at the capacitor of the output *LC* filter of the converter.
3) Dynamic reference frame (DRF): the DRF is slightly different from the previous two and is aligned with the control frequency—so we denote variables referenced to this rotating frame with superscript "*C*"—and has an angle θ_c that corresponds to the angle generated by the inertia-emulation loop, θ_{vsm}, in the case of the CCVSM and the angle of the PLL, θ_{pll}, in the case of the VCVSM. This reference frame can also be viewed as the local reference frame seen from the control system.

Fig. 6 represents the phasor diagram of the two VSM-controlled converters, where we illustrate the location where each rotating reference frame is aligned.

In relation to these rotating reference frames, special care must be taken when comparing the impedances obtained from the analytical equations and the simulation model. Usually, the latter is obtained by injecting a perturbation signal—either voltage or current—at the output of the converter and calculating the impedance matrix by dividing the voltage and current. These variables are measured in the *abc*-domain, and

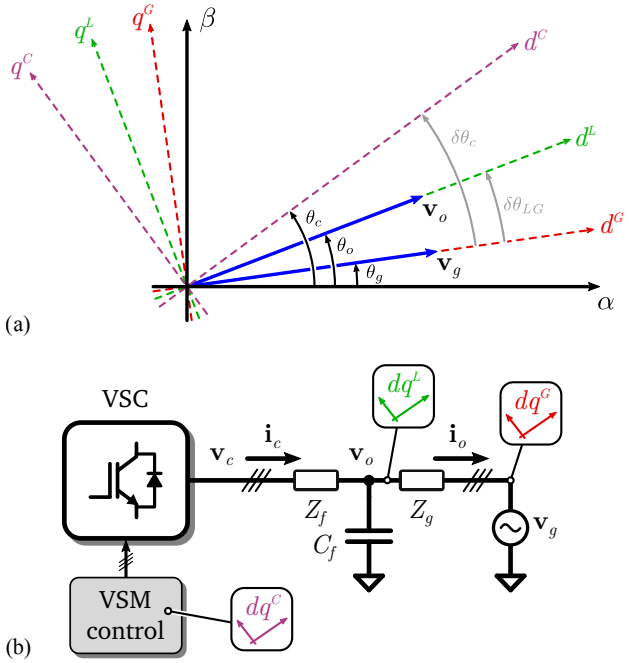

Fig. 6: Phasor diagram of VSM-controlled converter rotating reference frames.

are transformed into the LRF through a fast Fourier transform (FFT). If there is no impedance between the analyzed system and the grid, or if the power transmission between these two systems is zero, the LRF and the GRF are completely aligned. This means that the impedances referenced to any of these two rotating reference frames can be directly compared. However, when these two conditions are not met, the two rotating reference frames are not aligned any more due to the voltage drop in the impedance. As analytical impedances are most of the times referenced to the GRF, a rotation must be applied to one of the impedances so as to compare them in the same reference frame (step ⑥ in the proposed methodology). This is even more relevant when carrying out the impedance-based stability analysis of a system composed by multiple interconnected devices, as they must be all referenced to a common reference frame [23].

For the sake of simplicity and readability and due to space constraints we do not include the analytical development of the previously shown VSM-controlled converters. The reader is referred to [5] and [12] for the detailed equations of the CCVSM and the VCVSM, respectively.

The results shown in the next sections are obtained considering the following conditions:

1) The reactive power controllers are disabled by setting the reference q_{ref} and the droop gain K_q to zero in both cases.
2) No active damping loops are added in the control algorithms of converters, as they would influence their performance and stability characteristics. This means the analysis is done for non-augmented techniques, considering only their inherent behaviour.
3) All the analyzed systems begin the simulation from a

steady-state point of operation of $p = 0.5$ p.u. to reproduce a more realistic point of operation.

4) We model the delay of the PWM as a second order transfer function following the Padé approximation proposed in [24], which takes into account the computation delay, the sampler and the zero order hold and is modelled as a second order transfer function:

$$G_{pwm} = \frac{1 - 0.5T_s s}{(1 + 0.5T_s s)^2} \tag{1}$$

In addition, we must mention that the parameters used for the simulations are gathered from [5] and [12].

IV. Performance Evaluation of VSMs

In this section we evaluate the dynamic behaviour of VSM-controlled converters under different disturbances. These simulations serve not only to observe the response of each analyzed system but also to verify the analytical model by comparing it with the non-linear simulation model.

A. Active power reference variation

In this case we apply a step change in the active power reference, transitioning from $p_{\text{ref}} = 0.5$ p.u. to 0.6 p.u. The purpose of this simulation is to observe the response of the converter avoiding the effect of the frequency droop controller.

Fig. 7 shows the output power and frequency response of both cases for a 0.1 p.u. variation of the power reference $p_{m_{ref}}$.

The curves in this case show a very good accuracy between the non-linear and the developed small-signal models. Moreover, the CCVSM and VCVSM techniques show a similar behaviour; the difference resides in their overshooting and the time they require to reach the steady-state operation. However, this can be adapted by varying the emulated inertia and damping factor of the *swing equation* included in their control strategies.

B. Grid frequency variation

Here, the frequency of the grid begins at its rated value of 50 Hz and we apply a negative step variation of 0.2% of this rated frequency. This way we can study not only the dynamic behaviour but also the steady-state primary regulation of each system. The results are shown in Fig. 8.

In this case, the VCVSM technique has some overshooting and a small oscillation under the step variation, but it reaches the steady-state approximately in 0.5 s. On the other hand, the CCVSM has a very high overshoot ($\sim 30\%$) with no oscillation afterwards. Even though this can be problematic, CCVSM-controlled converters are very flexible and their response can be adapted by varying several control parameters. Moreover, despite its high overshooting, the CCVSM technique provides more inertial response compared to the VCVSM for the same H, which can be noticed by looking at the rate of change of frequency (RoCoF) of the curves shown at the right part of Fig. 8.

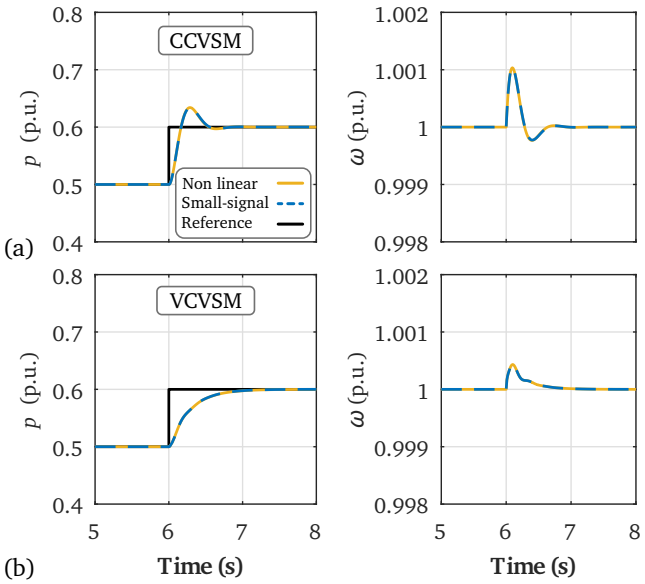

Fig. 7: Dynamic response of VSM-controlled converters under a power reference variation: (a) CCVSM and (b) VCVSM.

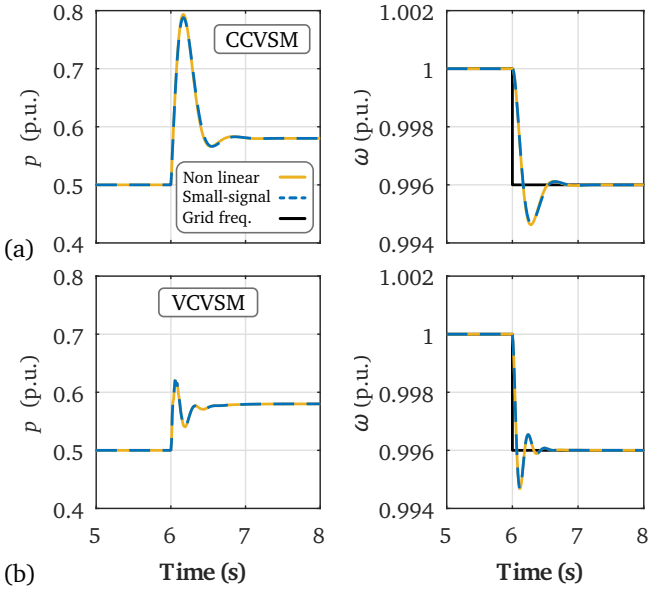

Fig. 8: Dynamic response of VSM-controlled converters under a grid frequency variation: (a) CCVSM and (b) VCVSM.

V. Impedance-Based Stability Analysis

Once we have verified the small-signal models in time-domain simulations and we have proven their performance under different types of perturbations, the next step is to study the stability of each system.

As we have already mentioned, in the literature there is a wide variety of methods to determine the stability of power electronic systems connected to ac grids. In this case we have decided to employ the generalized Nyquist criterion (GNC) following the process employed by Belkhayat in [20]

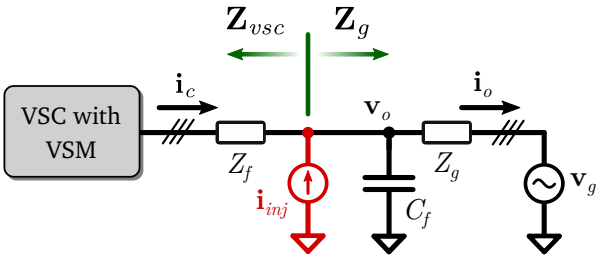

Fig. 9: Current injection point to measure the source and load impedances.

and by Burgos *et al.* in [21], which are based on the GNC theorem proposed by MacFarlane and Postlethwaite in [18] and [19]. With such method the stability of a closed-loop system can be determined by studying the location of the open-loop poles and encirclements of the $(-1+j0)$ point by the eigenvalues $\{\lambda_1, \lambda_2\}$ of the return-ratio matrix $\mathbf{L}_{dq}(s)$ (for the sake of simplicity the function of s is omitted in the notation, simplifying to $\mathbf{L}_{dq}$).

In order to obtain $\mathbf{L}_{dq}$, we need to extract the source ($\mathbf{Z}_{S_{dq}}$) and load impedances ($\mathbf{Z}_{L_{dq}}$) from the systems whose stability we want to analyze. In this context, we have assumed that the ideal voltage source, its series impedance, Z_g, and the capacitor C_f of the *LC* filter represent the source of the system and the VSC with its control and the output series Z_f impedance represent the load. This means that $\mathbf{Z}_{S_{dq}}$ corresponds to $\mathbf{Z}_g$ and $\mathbf{Z}_{L_{dq}}$ corresponds to $\mathbf{Z}_{vsc}$, as illustrated in Fig. 9.

We have derived the expressions of these impedances from the developed steady-state analytical models, splitting them into a source and load subsystem and calculating the transfer functions between the state variables and the inputs of the system.

Moreover, as we want to corroborate the correctness of these impedances prior to analyzing their stability, we have derived them not only by following the above-mentioned procedure, but also by measuring them in the simulations with the original non-linear systems. For the latter, we have employed a single-tone injection of current at the point where we split the source and the load (Fig. 9), following the procedure proposed by Rygg *et al.* in [25].

A. Output impedance comparative evaluation

Fig. 10 illustrates the frequency response of the impedances of the analyzed VSM techniques, as well as the equivalent grid impedance in black—which is equal in both cases.

The *dd* and *qq* terms of the CCVSM and VCVSM show an *RL* shape in most part of the frequency range, although the impedance of the VCVSM is more irregular than the CCVSM one. As we mentioned before, the VCVSM is more complex than the CCVSM, which has a direct impact on its impedance shape and stability characteristics. This can be clearly seen in the low frequency range (< 6 Hz), where the impedances of the VCVSM start showing a capacitive behaviour that could cause certain instabilities. This phenomenon is mainly caused by the use of a PLL for estimating the grid frequency, which means that if we generated this frequency internally as in the CCVSM, the shape of their impedances would be much closer.

We can say the impedances of the VSM techniques show a relatively clean shape in the entire frequency range. Moreover, the magnitude of their diagonal terms is higher than the grid impedance in most part of the frequency range, which is a desirable feature in terms of stability. One of the reasons for the higher magnitude impedances of these techniques is the virtual-impedances they integrate in the controllers. In the case of the CCVSM, for instance, these impedances could be adapted to emulate higher SM virtual windings in order to improve the stability characteristics of the overall system; however, this would also modify the dynamic response of the converter under disturbances, so we have to reach a compromise to ensure a correct operation.

In general, we can also see from Fig. 10 that at frequencies higher than 500 Hz the output filter of the converter is the dominating impedance, and the control techniques have less impact. In this range of frequencies the impedances of the converter interact with the grid side ones and their phase difference is greater than 100°, which could lead to weak stability characteristics as will be shown in the next section.

B. Stability analysis based on the generalized Nyquist criterion

Based on the impedances obtained in the previous section, here we derive the return-ration matrix $\mathbf{L}_{dq}$ and the eigenvalues of each system in order to analyze their stability with the generalized Nyquist criterion.

Fig. 11 illustrates the Nyquist plots of the two analyzed VSM-controlled converters.

The results of the CCVSM technique (Fig. 11(a)) show very good characteristics in terms of stability compared to the VCVSM strategy. The eigenvalues do not encircle the $(-1+j0)$ point and the system has an infinite gain margin—as the eigenvalues do not cross the negative part of the real axis—and a phase margin of 45.24°, which demonstrates that the system is very robust under parameter variations. In this case we can see that the frequency in which the eigenvalues cross the unity circle most near to the $(-1+j0)$ point is near 744 Hz. As previously mentioned this corresponds to the range close to the resonance of the filter capacitor and the grid side impedance.

On the other hand, the curves of the VCVSM (Fig. 11(b)) show that the system is very close to become unstable with a gain margin of 0.65 dB and a phase margin of 3.44°, determined by the second eigenvalue. The frequency of the point in which the eigenvalues—in this case λ_2—cross the unity circle most near to the $(-1+j0)$ point is nearly 1230 Hz, which means that the converter is interacting with the grid in this range of frequencies. Looking back at Fig. 10, we can see that this frequency corresponds to the case where Z_{qq} crosses with the grid side impedance. As in this case the off-diagonal terms of $\mathbf{Z}_{vsc_{dq}}$ are very low compared to the diagonal terms, we can say that Z_{qq} is closely related to λ_2. At this crossing point we can observe that both impedances have a high phase

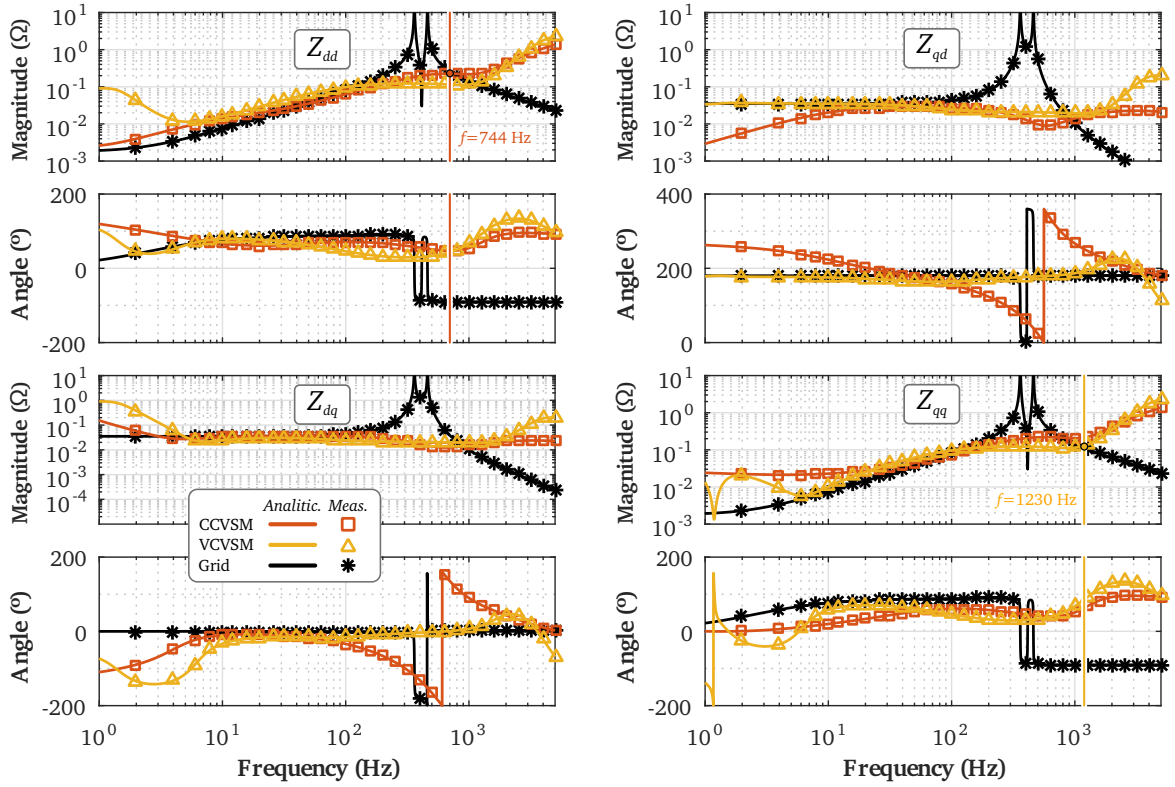

Fig. 10: *dq* domain output impedances of VSMs.

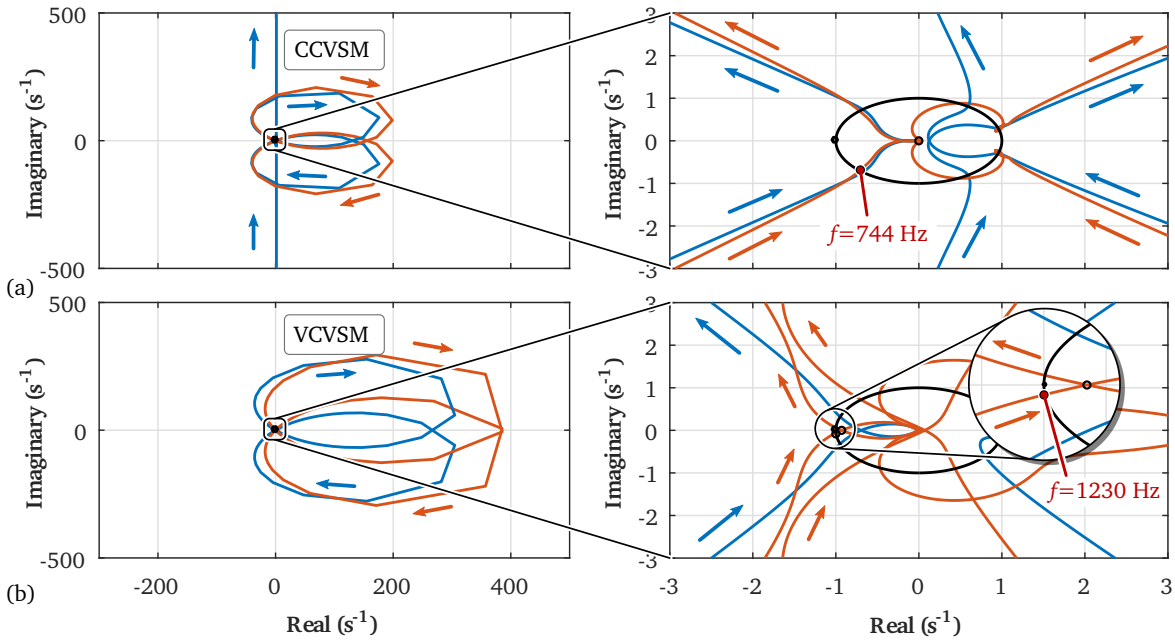

Fig. 11: Nyquist plots of VSM-controlled VSC eigenvalues: (a) Current-controlled VSM and (b) Voltage-controlled VSM.

difference, which is the source of these weak stability margins. Nevertheless, we must also take into account that even though in this case λ_1 shows better margins than λ_2, both eigenvalues have a similar shape and cross the unity circle at similar frequencies. This means that any of the two eigenvalues could cause the system to become unstable for variations in system parameters.

Looking at these results, we can conclude that a method for improving the stability margins not only of the VCVSM but also of the CCVSM might be the integration of active

damping loops in the regulators of the converter to dampen the resonances of the output filter of the converter, as it is done in [12]. This would modify the shape of the impedances so that their interaction ranges are changed to reduce the phase differences and increase the stability margins.

VI. Conclusion

In this paper we have carried out a comparative evaluation of current-controlled and voltage-controlled virtual synchronous machines in terms of performance and impedance-based stability.

The results show that even though the CCVSM and VCVSM have a similar dynamic response under power reference and grid frequency perturbations, their inherent stability characteristics are quite different. In this sense, we have observed that the shape of the impedances of VCVSM techniques is more irregular than in the CCVSM, mainly in the low frequency range. This difference is mainly caused by how the frequency of the grid is estimated, because the bandwidth of the PLL integrated in the VCVSM technique makes the impedances capacitive at this frequency range, which could be the source of instabilities at certain conditions. In any case, the CCVSM as well as the VCVSM show an *RL* shape for most part of the analyzed frequency range, and we have seen that at frequencies over 500 Hz the control techniques have less impact and the passive devices of the system become the dominant elements. Moreover, from the obtained Nyquist curves we can conclude that the stability margins of both techniques are determined by the interactions of the impedances at this range of frequencies. In this context, the CCVSM shows very good inherent characteristics in terms of stability compared to the VCVSM. However, we also believe the integration of active damping loops could significantly improve the stability margins of the latter by adapting the shape of its impedances in the range where they interact with the side of the grid. We leave this analysis opened for further research activities.

In this paper we have also developed a methodology where we highlight the importance of taking into account the rotating reference frame to which the impedances are aligned. In order to compare impedances obtained at different points of the ac grid, we need to shift them to a common reference frame applying a simple rotation matrix because of the voltage drops across line impedances.

Acknowledgment

This work has been partially funded by a predoctoral grant of the Basque Government (PRE_2016_2_0241)

References

[1] B. Kroposki, B. Johnson, Y. Zhang, V. Gevorgian, P. Denholm, B.-M. Hodge, and B. Hannegan, "Achieving a 100% Renewable Grid: Operating Electric Power Systems with Extremely High Levels of Variable Renewable Energy," *IEEE Power Energy Mag.*, vol. 15, no. 2, pp. 61–73, mar 2017.

[3] ——, "Hybrid ac/dc microgrids—Part II: Review and classification of control strategies," *Renew. Sustain. Energy Rev.*, vol. 52, pp. 1123–1134, dec 2015.

[2] E. Unamuno and J. A. Barrena, "Hybrid ac/dc microgrids—Part I: Review and classification of topologies," *Renew. Sustain. Energy Rev.*, vol. 52, pp. 1251–1259, dec 2015.

[4] ——, "Hybrid AC/DC Microgrid Mode-Adaptive Controls," in *Dev. Integr. Microgrids*, W.-P. Cao and J. Yang, Eds. InTech, 2017, ch. 11, pp. 255–273.

[5] O. Mo, S. D'Arco, and J. A. Suul, "Evaluation of Virtual Synchronous Machines with Dynamic or Quasi-stationary Machine Models," *IEEE Trans. Ind. Electron.*, vol. 0046, no. c, pp. 1–1, 2016.

[6] Q.-C. Zhong, Z. Ma, W.-L. Ming, and G. C. Konstantopoulos, "Grid-friendly wind power systems based on the synchronverter technology," *Energy Convers. Manag.*, vol. 89, pp. 719–726, jan 2015.

[7] S. D'Arco and J. A. Suul, "Virtual synchronous machines—Classification of implementations and analysis of equivalence to droop controllers for microgrids," in *2013 IEEE Grenoble Conf.* IEEE, jun 2013, pp. 1–7.

[8] H. Bevrani, T. Ise, and Y. Miura, "Virtual synchronous generators: A survey and new perspectives," *Int. J. Electr. Power Energy Syst.*, vol. 54, pp. 244–254, jan 2014.

[9] J. A. Suul, S. DArco, and G. Guidi, "Virtual Synchronous Machine-Based Control of a Single-Phase Bi-Directional Battery Charger for Providing Vehicle-to-Grid Services," *IEEE Trans. Ind. Appl.*, vol. 52, no. 4, pp. 3234–3244, jul 2016.

[10] R. Hesse, D. Turschner, and H.-P. Beck, "Micro grid stabilization using the Virtual Synchronous Machine (VISMA)," *2009 Int. Conf. Renew. Energies Power Qual.*, 2009.

[11] P. F. Frack, P. E. Mercado, M. G. Molina, E. H. Watanabe, R. W. De Doncker, and H. Stagge, "Control Strategy for Frequency Control in Autonomous Microgrids," *IEEE J. Emerg. Sel. Top. Power Electron.*, vol. 3, no. 4, pp. 1046–1055, dec 2015.

[12] S. D'Arco, J. A. Suul, and O. B. Fosso, "A Virtual Synchronous Machine implementation for distributed control of power converters in SmartGrids," *Electr. Power Syst. Res.*, vol. 122, pp. 180–197, 2015.

[13] D. J. Hogan, F. Gonzalez-Espin, J. G. Hayes, G. Lightbody, L. Albiol-Tendillo, and R. Foley, "Virtual synchronous-machine control of voltage-source converters in a low-voltage microgrid," in *2016 18th Eur. Conf. Power Electron. Appl. (EPE'16 ECCE Eur.* IEEE, sep 2016, pp. 1–10.

[14] Y. Hirase, K. Abe, K. Sugimoto, and Y. Shindo, "A grid-connected inverter with virtual synchronous generator model of algebraic type," *Electr. Eng. Japan*, vol. 184, no. 4, pp. 10–21, sep 2013.

[15] Y. Chen, R. Hesse, D. Turschner, and H.-p. Beck, "Comparison of methods for implementing virtual synchronous machine on inverters," in *Int. Conf. Renew. Energies Power Qual.*, 2012, pp. 1–6.

[16] H.-P. Beck and R. Hesse, "Virtual synchronous machine," in *2007 9th Int. Conf. Electr. Power Qual. Util.* IEEE, oct 2007, pp. 1–6.

[17] S. D'Arco and J. A. Suul, "Equivalence of virtual synchronous machines and frequency-droops for converter-based Microgrids," *IEEE Trans. Smart Grid*, vol. 5, no. 1, pp. 394–395, 2014.

[18] A. G. MacFarlane and I. Postlethwaite, "The generalized Nyquist stability criterion and multivariable root loci," *Int. J. Control*, vol. 25, no. 1, pp. 81–127, jan 1977.

[19] A. G. MacFarlane, *Frequency-Response Methods in Control Systems*. IEEE Press, 1979, vol. 3, no. 1.

[20] M. Belkhayat, "Stability Criteria for AC Power Systems with Regulated Loads," Ph.D. dissertation, 1997.

[21] R. Burgos, D. Boroyevich, F. Wang, K. Karimi, and G. Francis, "On the Ac stability of high power factor three-phase rectifiers," in *2010 IEEE Energy Convers. Congr. Expo.* IEEE, sep 2010, pp. 2047–2054.

[22] M. Amin, M. Molinas, J. Lyu, and X. Cai, "Impact of Power Flow Direction on the Stability of VSC-HVDC Seen From the Impedance Nyquist Plot," *IEEE Trans. Power Electron.*, vol. 32, no. 10, pp. 8204–8217, oct 2017.

[23] A. Rygg, M. Molinas, E. Unamuno, C. Zhang, and X. Cai, "A simple method for shifting local dq impedance models to a global reference frame for stability analysis," pp. 1–5, jun 2017.

[24] J. L. Agorreta, M. Borrega, J. López, and L. Marroyo, "Modeling and Control of N-Paralleled Grid-Connected Inverters With LCL Filter Coupled Due to Grid Impedance in PV Plants," *IEEE Trans. Power Electron.*, vol. 26, no. 3, pp. 770–785, mar 2011.

[25] A. Rygg, M. Molinas, Chen Zhang, and Xu Cai, "Frequency-dependent source and load impedances in power systems based on power electronic converters," in *2016 Power Syst. Comput. Conf.* IEEE, jun 2016, pp. 1–8.